Asian Journal of Chemistry; Vol. 34, No. 1 (2022), 201-208

ASIAN JOURNAL OF CHEMISTRY

https://doi.org/10.14233/ajchem.2022.23506

Fabrication of Magnetic Nanoparticles Integrated Carbon Matrix from *Chrysopogon zizanioides* Roots: Strong Dye Adsorption and Persulphate Assisted Photodegradation

A.P. Mary Sri Archana and A. Edwin Vasu*

Department of Chemistry, St. Joseph's College (Autonomous), Affiliated to Bharathidasan University, Tiruchirappalli-620002, India

*Corresponding author: E-mail: sjcvasu@gmail.com

Received: 31 August 2021; *Accepted*: 9 October 2021; *Published online*: 16 December 2021; AJC-20636

Activated carbon with magnetic nanoparticles was prepared from the roots of *Chrysopogon zizanioides* by impregnating the biomass with Fe^{3+} followed by carbonization in a muffle furnace. To assist the carbonization process, Zn^{2+} ions were also taken along with ferric ions during impregnation. The pH_{ZPC}, density of surface functional groups, surface acidity constants and advanced characterizations like FT-IR, N_2 adsorption-desorption isotherms, SEM with EDAX, DLS, XRD and VSM analysis were carried out. The adsorption and natural sunlight induced photooxidation of two cationic dyes, namely, methylene blue and rhodamine B in presence of potassium persulphate were studied by varying parameters like time, dye concentration, pH of the dye solution, amount of magnetic activated carbon and concentration of persulphate ions. The adsorption capacities of methylene blue and rhodamine B were found to be 5.97 and 0.96 mg/g, respectively. Photocatalytic oxidation of the dyes was very rapid in the presence of persulphate with the observed rate constants being 5.3×10^{-3} min^{-1} for methylene blue and 13.0×10^{-3} min^{-1} for rhodamine B. The magnetic activated carbon is found to be effective even after five successive degradation experiments.

Keywords: Magnetic activated carbon, Adsorption isotherm, Photodegradation, Methylene blue, Rhodamine B.

INTRODUCTION

Water is the most important and essential element for the sustenance of life on earth. Rapid growth of paper, textile, dyeing/printing industries, deteriorate the quality of the water resources as their effluents are contaminated with many coloured compounds, particularly dyes [1]. A number of cleanup methods are available for dyes from water [2,3] such as coagulation, flocculation, ion-exchange, advanced oxidation processes including photocatalytic degradation, adsorption and others. Adsorption by magnetic composite materials [4] is a promising technique, nowadays, as this easily separates the adsorbent from the effluent by an external magnet. In addition, magnetic carbons are also able to act as heterogenous photocatalysts for the oxidation organic compounds in a photo-Fenton like process in the presence of reagents like hydrogen peroxide or persulphate [5,6]. At present, magnetic carbon composites are mainly prepared from biomasses by a two-step method, which consists of carbonization followed by incorporation of magnetic character [7,8]. But such composites can also be prepared by having the magnetic precursor during carbonization, which is comparatively easier leaving composites with stable magnetic properties [9-11].

In present work, the magnetic vetiver carbon (MVC) has been prepared by impregnation of the biomass with ferric chloride followed by carbonization in muffle furnace. Zinc chloride is also taken along with the iron source during impregnation, for it can assist the carbonization process [12]. The composite was characterized by FT-IR, SEM with EDAX, DLS, BET, XRD and VSM studies. Methylene blue and rhodamine B dyes have been chosen as model dyes and their adsorption and sun light induced photodegradation on magnetic vetivar carbon (MVC) assisted by persulphate has been studied.

EXPERIMENTAL

All the reagents and chemicals used were of AR grade and used without further purification. Ferric chloride hexahydrate ($FeCl_3 \cdot 6H_2O$) 97% and rhodamine B dye were purchased from Loba Chemie Pvt. Ltd., whereas methylene blue dye, zinc

chloride and potassium persulphate were purchased from Merck Pvt. Ltd. Double distilled water was used to prepare all the solutions.

Synthesis of magnetic vetiver carbon (MVC): Roots of *Chrysopogon zizanioides* (vetiver) biomass were cut to pieces, washed with double distilled water and air dried. Zinc chloride (2 g) and $FeCl_3 \cdot 6H_2O$ (2 g) were added to 250 mL of deionized water and mixed uniformly using a magnetic stirrer. Then, 10 g of dried biomass was added to the solution and sonicated for 2 h. After the sonication, the contents were kept for 24 h, filtered, washed with water to remove excess metal ions and finally dried at 80 ºC in an air-oven. The dried roots were transferred into a porcelain container and pyrolyzed at 500 ºC in a muffle furnace for 0.5 h. After pyrolysis, the sample was naturally cooled to room temperature, washed with deionized water until the washings become neutral and dried at 80 ºC and stored.

Characterization: Cation-exchange capacity, pH_{ZPC} and densities of surface groups were determined by potentiometric titrations and boehm titrations [13,14]. Fourier transform infrared spectrum (FTIR) was recorded in Perkin Elmer, Spectrum Two model. Surface area was measured by N_2 adsorption-desorption measurements recorded in Thermo Fisher Scientific S.P.A., Italy, surface analyzer, S.No. SRFA13/0011.SEM images were taken on CAREL ZEISS Model EVO 18. XRD pattern was recorded in X'Pert Pro MPD, Panalytical, X-ray diffractometer using Cu$K\alpha$ radiation in order to analyze the diffraction pattern. Magnetic measurements were studied by vibrating sample magnetometer (VSM), Model Lake Shore 7400-S series. The elemental composition of the materials was determined by energy dispersive X-ray analysis (EDAX), Tescan Oxford. The size distribution of the particles in the composite was analyzed by particle size analyzer, Micromeritics, NanoPlus.

Adsorption of dyes in dark: The adsorption capacities of MVC were determined by dispersing them in 50 mL of dyes solutions in Erlenmeyer flasks in the dark. The initial (C_o) and final (C_e) concentrations of dye were analyzed using a Spectronic 20D+ spectrophotometer with absorption maximum at 665 nm for methylene blue and 555 nm for rhodamine B and the adsorption capacity was calculated using eqn. 1:

$$q_e = \frac{(C_o - C_e)V}{m} \quad (1)$$

where, q_e (mg g^{-1}) is the amount adsorbed at equilibrium, V (mL) is the volume of the reaction solution, m (g) is the mass of the dry adsorbent used for the adsorption study.

Photooxidation studies: For the photooxidation studies, after equilibrating 50 mL of dye solutions with MVC in the dark for 30 min, desired amounts of potassium persulphate and the solution is irradiated under natural sunlight with magnetic stirring. Aliquots of 2 mL were withdrawn periodically and analyzed for residual dye concentration (C_t, mg/L) at various times. A control without MVC is also carried out simultaneously. The amount of photodegradation was calculated from eqn. 2:

$$\text{Photodegradation } (\%) = \frac{(C_o - C_t)}{C_o} \times 100 \quad (2)$$

RESULTS AND DISCUSSION

Potentiometric and Boehm titrations: The point of zero charge (pH_{ZPC}) describes the condition when the electrical charge density on the surface is null. The surface acidity constants, pK_a^S and pH_{ZPC} were evaluated using potentiometric titrations following the method reported by Stumm & Morgan [15] and the results are shown in Table-1 along with Boehm titration results. Cation exchange capacity (CEC) is the measure of exchangeable sites available on the surface of the adsorbent for cations. The CEC for MVC is found to be 4.537×10^{-4} mol/g. The pK_a values indicate that MVC has strongly acidic groups on its surface. This may be attributed to the presence of acidic γ-Fe_2O_3 on its surface. The pH_{ZPC} value suggest that when MVC was introduced in neutral aqueous solution; its surface will acquire negative charge and thus will have increased affinity towards cations like methylene blue and rhodamine B. The results of Boehm titrations show that MVC has significant amounts of acidic groups on its surface with relatively smaller numbers of basic groups. These results were in accordance to low pK_a value of 2 as quoted by the potentiometric titrations.

TABLE-1
POTENTIOMETRIC AND BOEHM TITRATIONS

Potentiometric titration results		Density of surface groups (meq/g)	
CEC (mol/g)	4.537×10^{-4}	Carboxyl	0.115
pK_{a1}^S	2	Phenolic	0.110
pK_{a2}^S	9.4	Lactonic	0.045
pH_{ZPC}	5.7	Acidic groups	0.270
		Basic groups	0.015
		Total groups	0.285

FTIR studies: Fig. 1 shows the FTIR spectrum of MVC. A strong broad band at 3433.12 cm^{-1} is characteristic of –OH group of carboxylic acids [11]. The strong peak at 1614.84 cm^{-1} could be attributed to C=C vibrations, which indicates the aromatic rings in biochar [16]. Peaks at 1115.29 and 1052.86 cm^{-1} are attributed to C–O stretching vibrations. Iron in the composite was evidenced from the peak at 542 cm^{-1} which is due to the Fe–O stretching, indicating the presence of iron oxides in the carbon matrix [16,17].

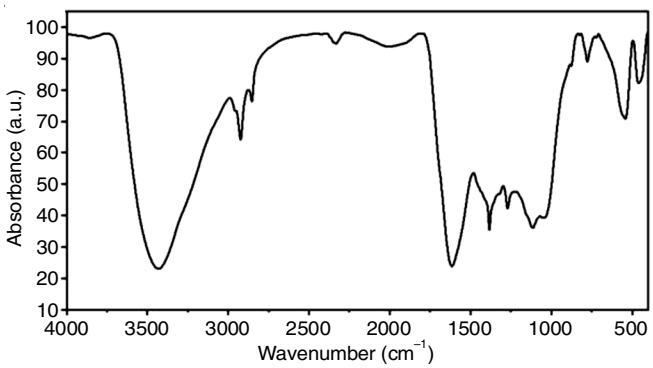

Fig. 1. FTIR spectrum of magnetic vetivar carbon (MVC)

SEM studies: The SEM images of MVC are shown in Fig. 2a-f. Fig. 2a reveals that the carbon matrix has a layer-like structure with numerous pores on its surface. Fig. 2b-e

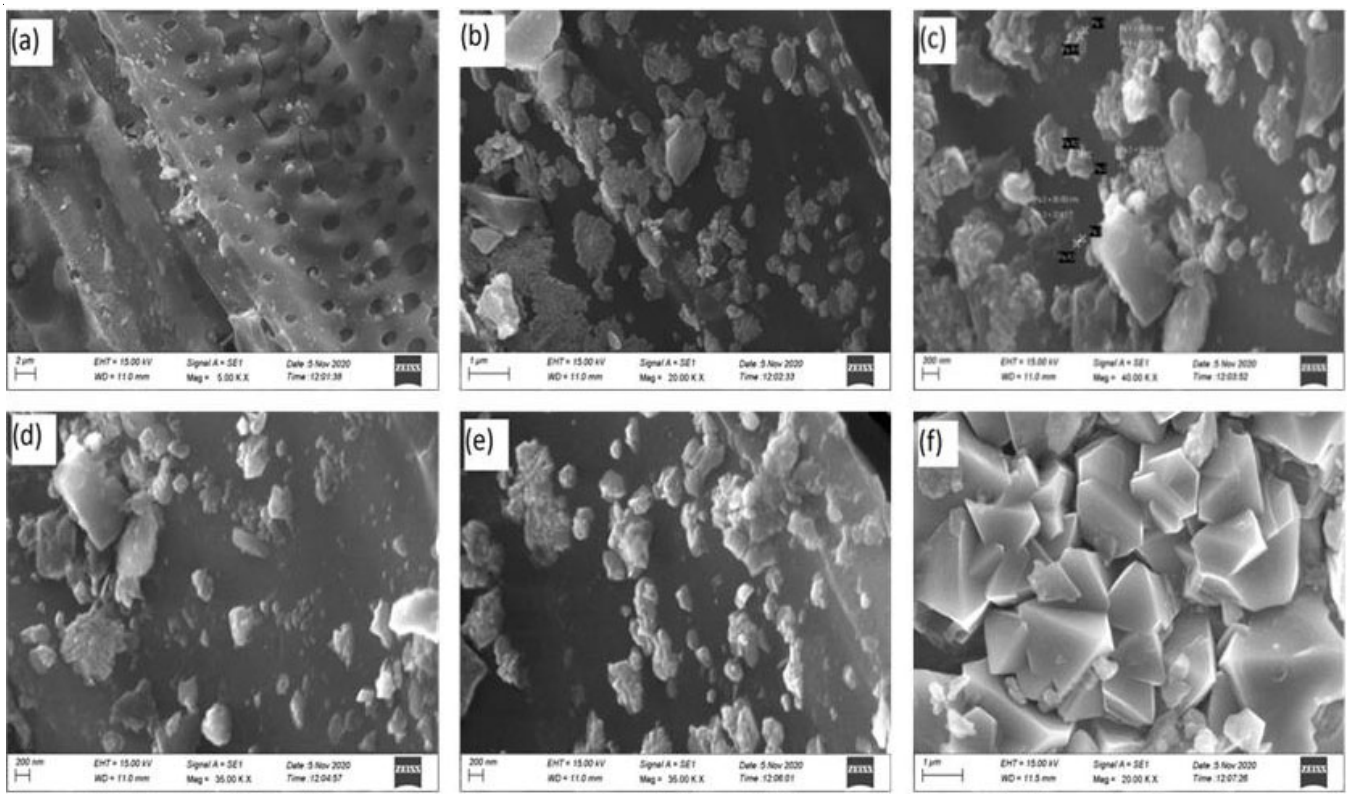

Fig. 2. (a-f) SEM images of magnetic vetiver carbon (MVC)

show a good dispersion of iron oxide clusters on the surface of the carbon matrix and Fig. 2f clearly depicts the cubic crystals of iron oxide that are found to be embedded on the carbon matrix. The EDAX spectrum confirms the presence of carbon, oxygen and iron in large amounts with traces of zinc, chlorine and silicon (Fig. 3). Iron is present in 5.23% by weight which depicts the successful impregnation of iron onto the composite.

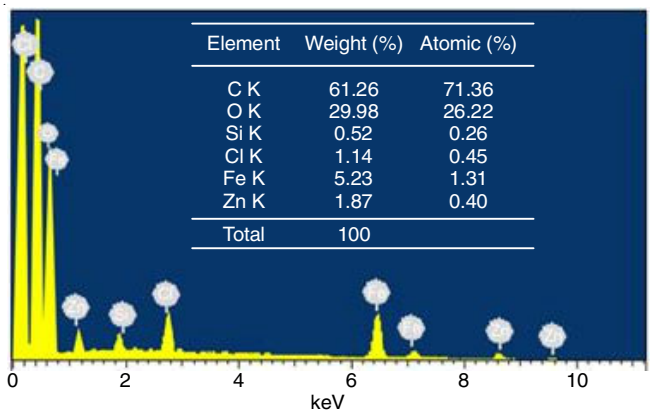

Fig. 3. EDAX spectrum of magnetic vetiver carbon (MVC)

BET surface area studies: The textural properties of the adsorbent were investigated by N_2 adsorption and desorption measurements. The isotherm of MVC could be classified as Type I (Langmuir type) which is a characteristic of micro-porous materials [18] (Fig. 4). The specific surface area was 91.3252 $m^2 g^{-1}$ with specific pore volume of 0.0552 $cm^3 g^{-1}$. The value of surface area is in agreement to the large particle

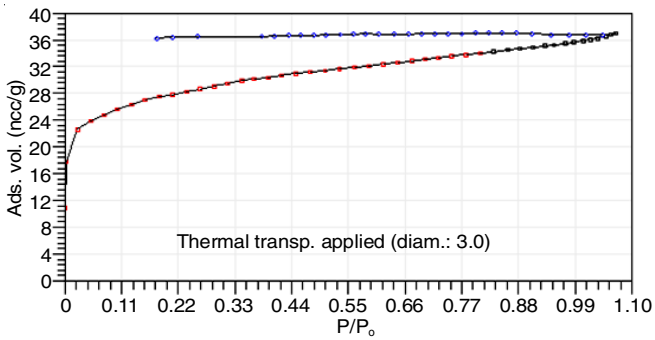

Fig. 4. N_2 adsorption-desorption isotherm on magnetic vetivar carbon (MVC)

size of 363.7 nm as observed in the dynamic light scattering (DLS) results (Table-2). The slightly low value of surface area may be attributed due to the presence of iron oxide-based particles occupying some of the void spaces in the material [19]. But it is worth to note that the synthesized MVC has comparable surface area to some related materials that were previously reported. For instance, the surface area of a copper oxide loaded activated carbon prepared in one step [20] has a surface area of 83 $m^2 g^{-1}$.

XRD studies: The XRD pattern of MVC is presented in Fig. 5. The broad assymmetric peaks from 2θ = 12º to 29º indicates that MVC is a typical amorphous carbon [21]. The

TABLE-2
DYNAMIC LIGHT SCATTERING RESULTS

Diameter (d)	363.7 nm
Polydispersity index (P.I.)	0.253
Diffusion const. (D)	1.352e-008 (cm^2/s)

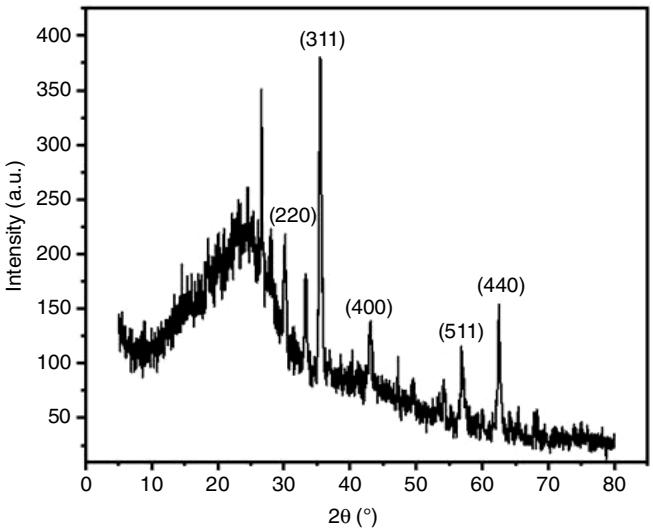

Fig. 5. XRD pattern of magnetic vetivar carbon (MVC)

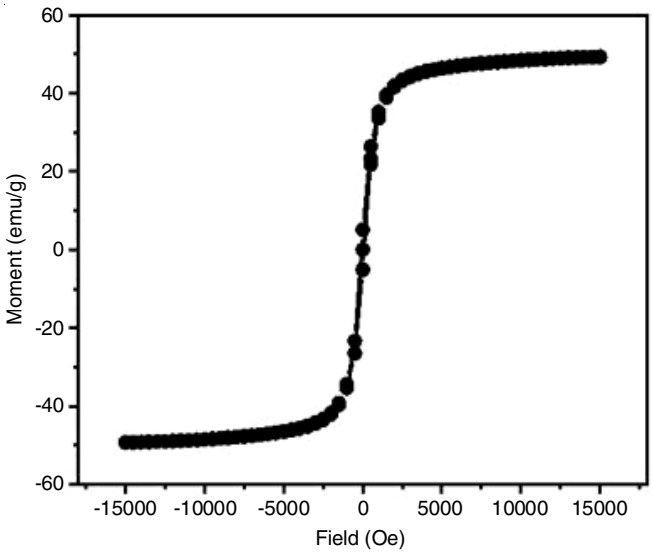

Fig. 6. VSM magnetization curve of magnetic vetivar carbon (MVC)

characteristic diffraction peak at 2θ = 26.4º is attributed to the plane of partially graphitized carbon material [22-24]. The diffraction peaks at 2θ = 30.2º, 35.5º, 43.2º, 56.8º and 62.5º correspond to the five indexed planes (220), (311), (400), (511) and (440) of maghemite (γ-Fe_2O_3), respectively [25]. This indicates that the iron oxides embedded in the carbon matrix are γ-Fe_2O_3, which has cubic structure of inverse spinel type [19]. These cubic structures of γ-Fe_2O_3 has occupied the surface of the carbon matrix as seen in the SEM images of Fig. 2f.

Magnetic properties: Magnetic characterizations were done at 300 K by ranging the magnetic field from -15000 O_e to +15000 O_e and the corresponding response of MVC has been recorded (Fig. 6). The strong magnetic curve has saturation near 50 emu g^{-1} and this amount of magnetization of MVC is sufficient enough to separate the composite in a very effective manner using an external magnet and is also comparable with results already reported [26]. The small hysteresis loop forms an additional evidence for the presence of iron oxide particles on to the carbon matrix as clearly visible in SEM images [27].

Adsorption isotherms: Three models were used in this study to model the adsorption of dyes on MVC, namely, Langmuir (eqn. 3), Freundlich (eqn. 4) and Redlich-Peterson (eqn. 5):

$$q_e = \frac{Q_{max} K_L C_e}{1 + K_L C_e} \quad (3)$$

$$q_e = K_F (C_e)^{1/n} \quad (4)$$

$$q_e = \frac{K_R C_e}{1 + b_R C_e^{\beta}} \quad (5)$$

where q_e (mg g^{-1}) is the amount adsorbed per gram of the adsorbent at equilibrium, C_e (mg L^{-1}) is the equilibrium concentration of the adsorbate, Q_{max} (mg g^{-1}) is the Langmuir monolayer capacity, K_L is the Langmuir isotherm constant, where n is the adsorption intensity, K_F is the Freundlich isotherm constant and K_R, b_R and β are constants involved in the Redlich-Peterson isotherm. The adsorption behaviours are shown in Fig. 7a (for

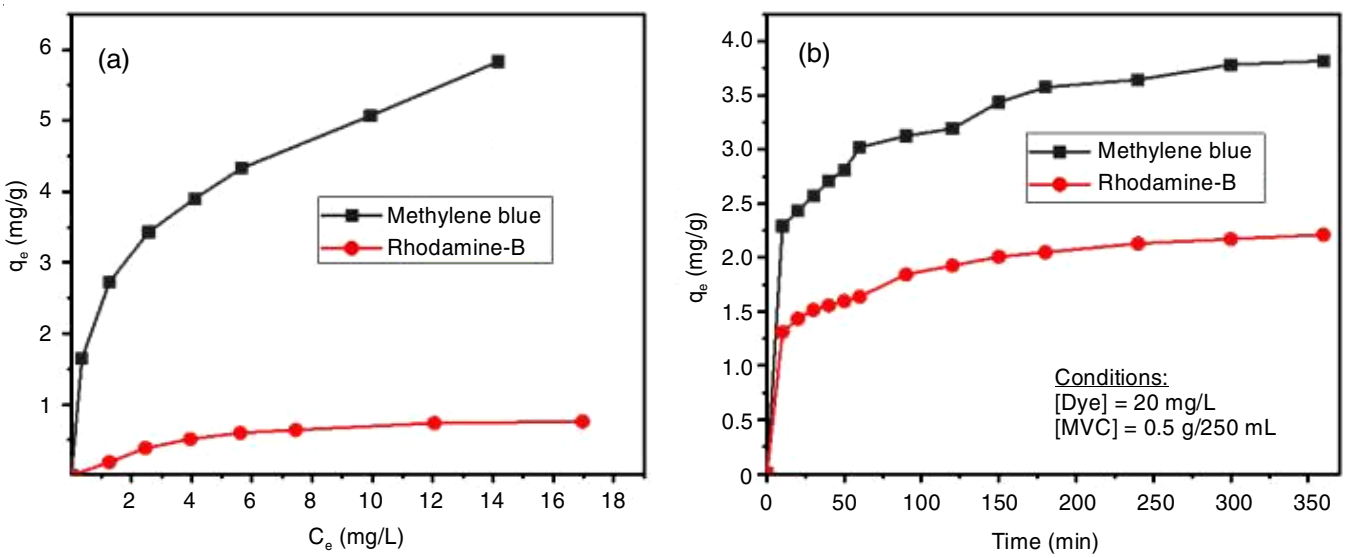

Fig. 7. Adsorption isotherms (a) and kinetic curves (b) for the adsorption of methylene blue and rhodamine B on magnetic vetivar carbon (MVC)

methylene blue: C_i = 2 to 20 mg/L, MVC dose = 0.05 g/50 mL, contact time = 24 h; for rhodamine B: C_i = 2 to 20 mg/L, MVC dose = 0.2 g/50 mL, contact time = 24 h) and the data is fitted with the three isotherm equations and the results are presented in Table-3. The r^2 values obtained show that the three-parameter Redlich-Peterson model is the best.

Kinetic aspects: In order to analyze the kinetics behaviour of the dyes on the adsorbent; two kinetic models; Lagergren's pseudo-first order model (eqn. 6) and pseudo-second order model (eqn. 7) were used to fit the experimental kinetic data (Fig. 7b):

$$\log (q_{e(1)} - q_t) = \log q_e - k_1 t \quad (6)$$

$$\frac{t}{q_t} = \frac{1}{h} + \frac{t}{q_e^2} \quad (7)$$

where k_1 (min^{-1}) and k_2 (g mg^{-1} min^{-1}) are the rate constants of the pseudo-first order and pseudo-second order model respectively; q_t (mg g^{-1}) is the amount of dye adsorbed on the adsorbent at time t; h (= $k_2 q_e^2$, mg g^{-1} min^{-1}) is the initial sorption rate. The kinetic parameters obtained are listed in Table-4 and the correlation coefficient values suggest that the second order model, which describes the adsorption better.

Photooxidation studies: Preliminary studies reveal that there is significant photooxidation of the dyes in presence of MVC and the absorption spectra of the dyes proving their degradation are shown in Fig. 8. Iron oxide nanoparticles and iron oxide loaded activated carbon materials are known to produce sulphate radical ions in aqueous medium, which are able to oxidize many organic compounds and dyes. Ferrous ions either from the iron oxide matrix or those generated *in situ* from the solid in presence of sunlight [28] and also ferric ions are able to produce sulphate radical ions which are able to degrade a variety of organic compounds including phenol [28], rhodamine B [29], tetracycline [30], methylene blue [31] and others:

$$Fe^{2+} + S_2O_8^{2-} \longrightarrow Fe^{3+} + SO_4^{\bullet-} + SO_4^{2-} \quad (8)$$

$$SO_4^{\bullet-} + H_2O \longrightarrow OH^{\bullet} + HSO_4^{-} \quad (9)$$

$$SO_4^{\bullet-} + \text{Dye} \longrightarrow \text{Degradation products} \quad (10)$$

$$OH^{\bullet} + \text{Dye} \longrightarrow \text{Degradation products} \quad (11)$$

Kinetics of the photodegradation were done by the pseudo-first order model rate expression [32] in terms of eqn. 12:

$$\ln \frac{C_t}{C_o} = -k_{obs} t \quad (12)$$

The % degradation of methylene blue and rhodamine B in sunlight, assisted by potassium persulfate (PPS) with and without MVC is shown in Fig. 9a along with the kinetic plots in Fig. 9b. It is evident from Fig. 9a that addition of MVC greatly enhances the degradation of dyes. Within 30 min, the degradation efficiencies of methylene blue and rhodamine B increased from 11.27 to 23.24% and from 14.87 to 26.67%, respectively, in the presence of MVC. More than 80% degradation of 15 mg/L dye solutions were achieved at 120 min. The apparent rate constant obtained also confirm the enhanced degradation of dyes. The rate constant for methylene blue degradation increased from 1.9×10^{-3} to 5.3×10^{-3} min^{-1} and that of rhodamine B increased from 5.3×10^{-3} to 13.0×10^{-3} min^{-1} (Fig. 9b).

Effect of variables on photooxidation: The effect of variables like concentration of MVC, concentration of PPS, pH and degradation performances of MVC for five number of cycles are done and the results are presented in Fig. 10a-d. Concentrations of MVC were varied from 0.5 g/L to 1.5 g/L. Increase in MVC initially lead to greater reduction in dye concentrations and ultimately the degradations tend to be become saturated

TABLE-3
ISOTHERM CONSTANTS FOR ADSORPTION OF DYES ON MAGNETIC VETIVER CARBON (MVC)

Dye	Langmuir		Freundlich		Redlich-Peterson	
Methylene blue	K_L	0.5994	K_F	2.4702	K_R	29.8215
	b	0.1004	n	3.1057	b_R	11.0704
	Q_{max} (mg g^{-1})	5.9707	1/n	0.3220	β	0.7083
	r^2	0.9141	r^2	0.9962	r^2	0.9973
Rhodamine B	K_L	0.2670	K_F	0.2735	K_R	0.1913
	b	0.2790	n	2.5646	b_R	0.0898
	Q_{max} (mg g^{-1})	0.9570	1/n	0.3899	β	1.2729
	r^2	0.9759	r^2	0.8776	r^2	0.9882

TABLE-4
KINETIC PARAMETERS FOR ADSORPTION OF DYES ON MAGNETIC VETIVER CARBON (MVC)

Dye	First order		Second order	
Methylene blue	$q_{e(exp)}$ (mg g^{-1})	4.2708	$q_{e(exp)}$ (mg g^{-1})	4.2708
	$q_{e(1)}$ (mg g^{-1})	1.8126	$q_{e(2)}$ (mg g^{-1})	3.9574
	k_1 (min^{-1})	1.89×10^{-3}	k_2 (g $mg^{-1}min^{-1}$)	1.397×10^{-2}
	r^2	0.9544	h (mgg^{-1} min^{-1})	0.2188
			r^2	0.9973
Rhodamine B	$q_{e(exp)}$ (mg g^{-1})	2.6223	$q_{e(exp)}$ (mg g^{-1})	2.6223
	$q_{e(1)}$ (mg g^{-1})	1.1800	$q_{e(2)}$ (mg g^{-1})	2.2920
	k_1 (min^{-1})	2.42×10^{-3}	k_2 (g $mg^{-1}min^{-1}$)	2.42×10^{-2}
	r^2	0.9303	h (mgg^{-1} min^{-1})	0.1272
			r^2	0.9979

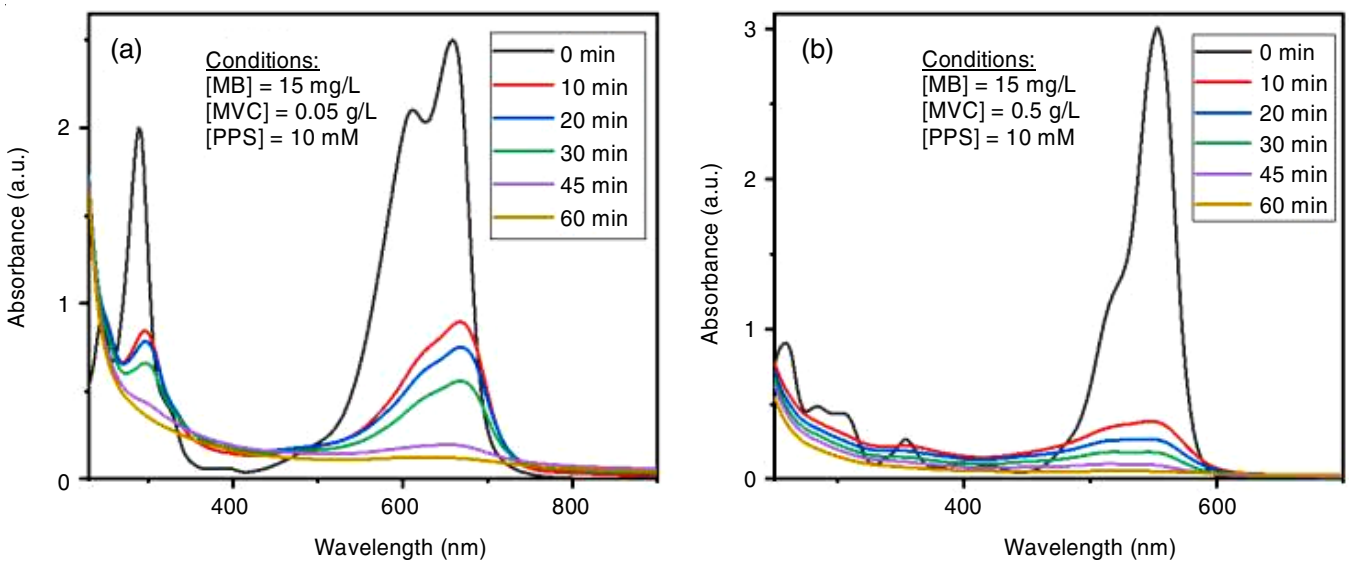

Fig. 8. UV-Visible spectra of photodegradation of methylene blue (a) and rhodamine B (b)

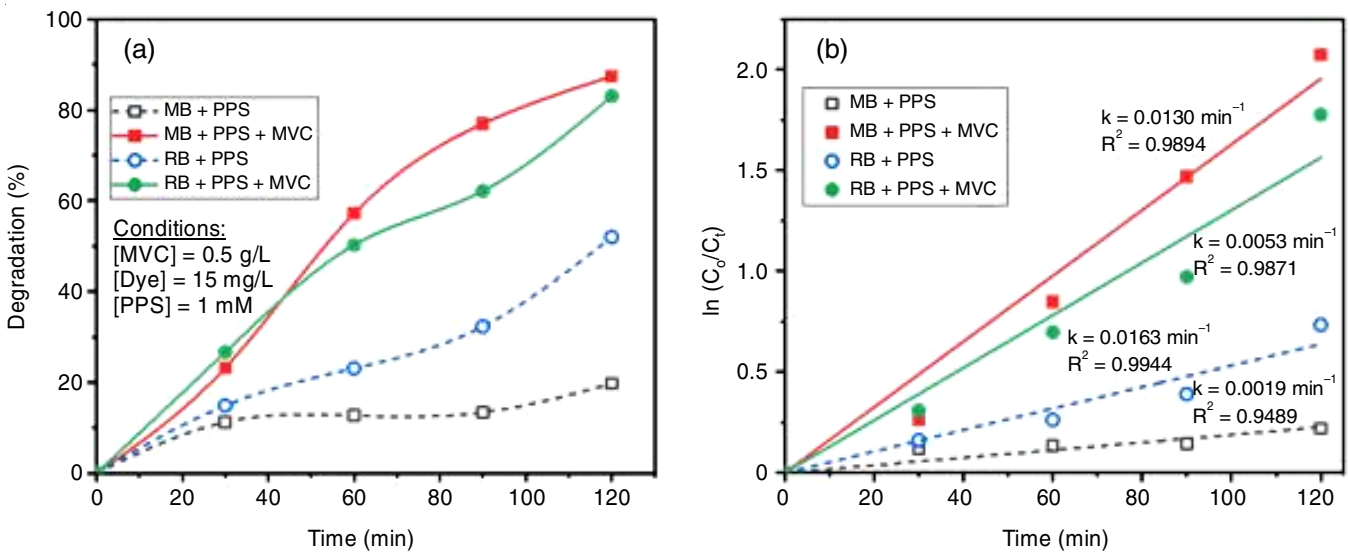

Fig. 9. Photodegradation kinetics of methylene blue and rhodamine B on magnetic vetivar carbon (MVC)

when 1.5 g/L MVC was used. It is to be noted that the time required for complete decolourization goes higher at increased MVC concentrations. For example, for rhodamine B, it takes 150 min for complete colour removal with 0.5 g/L MVC and only 125 and 90 min with 1.0 and 1.5 g/L MVC. The steep raise in the performance supports the greater number active species that are produced from the magnetic carbon. As far as the variation in the concentration of PPS is concerned, performances increased rapidly from 1 mM to 5 mM but further increase does not greatly change the degradation. Acidic pH generally found to increase the degradation performance of MVC over both the dyes (Fig. 10c). This is acceptable because ferrous and ferric ions activity can only be realized in acidic media, where as basic media generally inactivate them by means of precipitation. To test the applicability of MVC for practical situations, five number of degradation experiments were performed with the catalyst being regenerated after each performance by repeatedly washing with water and drying at 120 ºC. The results (Fig. 10d) show that not much change in the capacity even after five cycles. The slight decreases obtained could be due to loss of MVC or loss of active sites during the operations.

Comparison of MVC with other photocatalysts: Finally, an attempt has been made to compare the degradation capacity of MVC in terms of the first order rate constant with other catalysts that are reported in recent years (Table-5). It appears that its capacities are comparable with some nano composites and can be successfully used for the decolourization of wastewaters containing methylene blue and rhodamine B dyes.

Conclusion

In this work, magnetic vetiver carbon has been synthesized by a simple impregnation-carbonization procedure. Reasonable magnetic moment of the composite as evident in the VSM studies helps the separation of the adsorbent from dye effluent using an external magnet. The surface morphology, functional

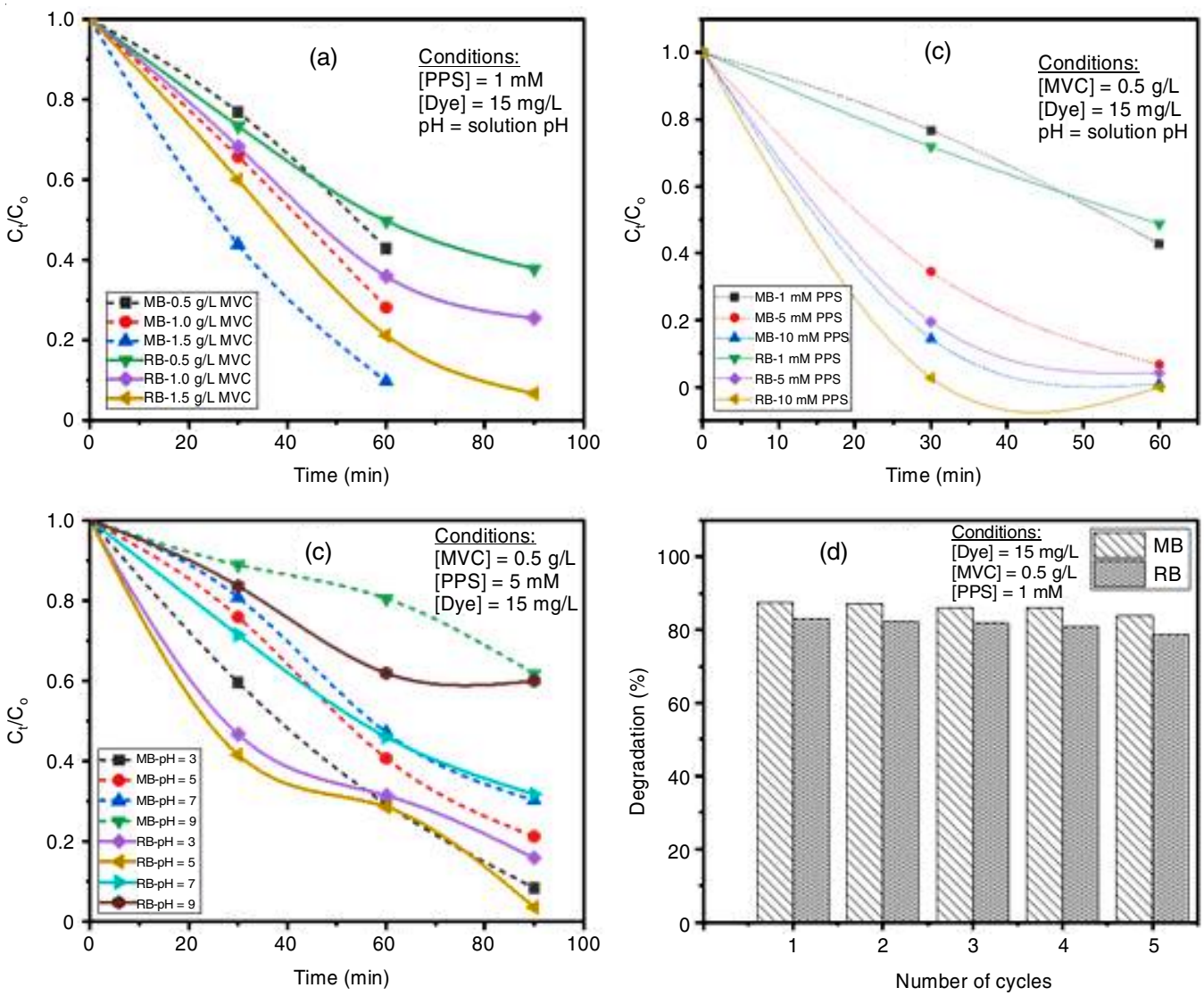

Fig. 10. Effect of magnetic vetiver carbon (MVC) concentration (a), persulphate concentration (b), pH (c) and number of cycles of operation on the photocatalytic degradation of methylene blue and rhodamine B (d)

TABLE-5
COMPARISON OF PHOTOCATALYTIC PERFORMANCE OF MAGNETIC VETIVER CARBON (MVC) WITH OTHER CATALYSTS

Dye	[Dye] (mg/L)	Photocatalyst	[Catalyst] (g/L)	Light source	$k \times 10^{-3}$ min^{-1}	Ref.
Methylene blue	50	GaN-ZnO/g-C_3N_4	0.500	75 W lamp	16.7	[33]
	40	PoPD-modified TiO_2 nanocomposite	0.030	1000 W xenon lamp	0.80-2.3	[34]
	3.2	$MnTiO_3$ nanoparticles	0.100	Sunlight	5.25	[35]
	15	Vetiver biomass derived magnetic carbon	0.500	Sun light	5.3	Present work
Rhodamine B	20	Fe-Cd co-doped ZnO nanoparticle	0.100	300W Xe lamp	9.16	[36]
	40	Biomass derived activated carbon supported CdS nanomaterials	0.200	300 W Xe arc lamp	24.0	[37]
	6	Zinc oxide activated charcoal polyaniline nanocomposite	1.000	Compact fluorescent lamp	31.0	[38]
	15	Vetiver biomass derived magnetic carbon	0.500	Sun light	13.0	Present work

groups, surface area, surface properties are characterized by SEM with EDAX, FTIR, BET and XRD studies. The adsorption capacity of MVC was tested with cationic dyes methylene blue and rhodamine B from aqueous solutions and it was also found to act as an efficient photocatalyst for the degradation of these dyes in presence of persulphate and sunlight. Photocatalytic efficiencies of 87.42% and 83.08%, for methylene blue and rhodamine B, respectively, were found when 15 mg/L dyes solutions were irradiated in sunlight in presence of 1 mM persulphate and 0.5 g/L MVC. The catalyst retained its activity after five complete cycles of performances.

CONFLICT OF INTEREST

The authors declare that there is no conflict of interests regarding the publication of this article.

REFERENCES

1. B. Lellis, C.Z. Favaro-Polonio, J.A. Pamphile and J.C. Polonio, *Biotechnol. Res. Innov.*, **3**, 275 (2019); https://doi.org/10.1016/j.biori.2019.09.001
2. S. Sharma and A. Kaur, *Indian J. Sci. Technol.*, **11**, 1 (2018); https://doi.org/10.17485/ijst/2018/v11i12/120847
3. S. Dutta, B. Gupta, S.K. Srivastava and A.K. Gupta, *Mater. Adv.*, **2**, 4497 (2021); https://doi.org/10.1039/D1MA00354B
4. R. Sivashankar, A.B. Sathya, K. Vasantharaj and V. Sivasubramanian, *Environ. Nanotechnol. Monit. Manag.*, **1-2**, 36 (2014); https://doi.org/10.1016/j.enmm.2014.06.001
5. M.C. Pereira, L.C.A. Oliveira and E. Murad, *Clay Miner.*, **47**, 285 (2012); https://doi.org/10.1180/claymin.2012.047.3.01
6. C. Dong, C. Chen and C. Hung, *Environ. Sci. Pollut. Res. Int.*, **26**, 33781 (2019); https://doi.org/10.1007/s11356-018-2423-2
7. S. Wang, Y. Tang, K. Li, Y. Mo, H. Li and Z. Gu, *Bioresour. Technol.*, **174**, 67 (2014); https://doi.org/10.1016/j.biortech.2014.10.007
8. M. Jain, M. Yadav, T. Kohout, M. Lahtinen, V.K. Garg and M. Sillanpaa, *Water Resour. Ind.*, **20**, 54 (2018); https://doi.org/10.1016/j.wri.2018.10.001
9. S. Zhang, L. Tao, M. Jiang, G. Gou and Z. Zhou, *Mater. Lett.*, **157**, 281 (2015); https://doi.org/10.1016/j.matlet.2015.05.117
10. M. Zhang, B. Gao, S. Varnoosfaderani, A. Hebard, Y. Yao and M. Inyang, *Bioresour. Technol.*, **130**, 457 (2013); https://doi.org/10.1016/j.biortech.2012.11.132
11. Z. Yin, Y. Liu, S. Liu, L. Jiang, X. Tan, G. Zeng, M. Li, S. Liu, S. Tian and Y. Fang, *Sci. Total Environ.*, **639**, 1530 (2018); https://doi.org/10.1016/j.scitotenv.2018.05.130
12. P.E. Hock and M.A.A. Zaini, *Acta Chim. Slov.*, **11**, 99 (2018); https://doi.org/10.2478/acs-2018-0015
13. M. Davranche, S. Lacour, F. Bordas and J.-C. Bollinger, *J. Chem. Educ.*, **80**, 76 (2003); https://doi.org/10.1021/ed080p76
14. R. Kummert and W.J. Stumm, *J. Colloid Interface Sci.*, **75**, 373 (1980); https://doi.org/10.1016/0021-9797(80)90462-2
15. W. Stumm and J.J. Morgan, Aquatic Chemistry, Chemical Equilibria and Rates in Natural Waters, Wiley: New York, Edn. 3 (1996).
16. M.A. Jadidi Kouhbanani, N. Beheshtkhoo, A.M. Amani, S. Taghizadeh, V. Beigi, A. Zakeri Bazmandeh and N. Khalaf, *Mater. Res. Express*, **5**, 115013 (2018); https://doi.org/10.1088/2053-1591/aadde8
17. G.Y. Li, Y.R. Jiang, K.I. Huang, P. Ding and J. Chen, *J. Alloys Compd.*, **466**, 451 (2008); https://doi.org/10.1016/j.jallcom.2007.11.100
18. A.L. Cazetta, O. Pezoti, K.C. Bedin, T.L. Silva, A. Paesano Junior, T. Asefa and V.C. Almeida, *ACS Sustain. Chem. Eng.*, **4**, 1058 (2016); https://doi.org/10.1021/acssuschemeng.5b01141
19. L.C.A. Oliveira, R.V.R.A. Rios, J.D. Fabris, V. Garg, K. Sapag and R.M. Lago, *Carbon*, **40**, 2177 (2002); https://doi.org/10.1016/S0008-6223(02)00076-3
20. M. Ghaedi, A.M. Ghaedi, M. Hossainpour, A. Ansari, M.H. Habibi and A.R. Asghari, *J. Ind. Eng. Chem.*, **20**, 1641 (2014); https://doi.org/10.1016/j.jiec.2013.08.011
21. K.T. Wong, Y. Yoon, S.A. Snyder and M. Jang, *Chemosphere*, **152**, 71 (2016); https://doi.org/10.1016/j.chemosphere.2016.02.090
22. B. Wang, Y. Jiang, F. Li and D. Yang, *Bioresour. Technol.*, **233**, 159 (2017); https://doi.org/10.1016/j.biortech.2017.02.103
23. D. Gholamvaisi, S. Azizian and M. Cheraghi, *J. Dispers. Sci. Technol.*, **35**, 9 (2014); https://doi.org/10.1080/01932691.2013.843465
24. M.T.H. Siddiqui, S. Nizamuddin, H.A. Baloch, N.M. Mubarak, D.K. Dumbre, Inamuddin, A.M. Asiri, A.W. Bhutto, M. Srinivasan and G.J. Griffin, *Environ. Chem. Lett.*, **16**, 821 (2018); https://doi.org/10.1007/s10311-018-0724-9
25. L. Machala, J. Tucek and R. Zboril, *Chem. Mater.*, **23**, 3255 (2011); https://doi.org/10.1021/cm200397g
26. S. Nethaji, A. Sivasamy and A.B. Mandal, *Bioresour. Technol.*, **134**, 94 (2013); https://doi.org/10.1016/j.biortech.2013.02.012
27. Y. Si, T. Ren, Y. Li, B. Ding and J. Yu, *Carbon*, **50**, 5176 (2012); https://doi.org/10.1016/j.carbon.2012.06.059
28. P. Avetta, A. Pensato, M. Minella, M. Malandrino, V. Maurino, C. Minero, K. Hanna and D. Vione, *Environ. Sci. Technol.*, **49**, 1043 (2015); https://doi.org/10.1021/es503741d
29. M.N. Pervez, W. He, T. Zarra, V. Naddeo and Y. Zhao, *Water*, **12**, 733 (2020); https://doi.org/10.3390/w12030733
30. V. Nguyen, C. Hung, T. Nguyen, J. Chang, T. Wang, C. Wu, Y. Lin, C. Chen and C. Dong, *Catalysts*, **9**, 49 (2019); https://doi.org/10.3390/catal9010049
31. C.M. Hung, C. Chen, Y. Jhuang and C. Dong, *J. Adv. Oxid. Technol.*, **19**, 43 (2016); https://doi.org/10.1515/jaots-2016-0105
32. W. Tsai, M. Lee, T. Su and Y. Chang, *J. Hazard. Mater.*, **168**, 269 (2009); https://doi.org/10.1016/j.jhazmat.2009.02.034
33. K. Nguyen Van, V.N. Nguyen Thi, T.P. Tran Thi, T.T. Truong, T. Lieu Le Thi, H. Tran Huu, V.T. Nguyen and V. Vo, *Chem. Phys. Lett.*, **763**, 138191 (2021); https://doi.org/10.1016/j.cplett.2020.138191
34. C. Yang, W. Dong, G. Cui, Y. Zhao, X. Shi, X. Xia, B. Tang and W. Wang, *Sci. Rep.*, **7**, 3973 (2017); https://doi.org/10.1038/s41598-017-04398-x
35. S. Alkaykh, A. Mbarek and E.E. Ali-Shattle, *Heliyon*, **6**, e03663 (2020); https://doi.org/10.1016/j.heliyon.2020.e03663
36. D. Neena, K.K. Kondamareddy, H. Bin, D. Lu, P. Kumar, R.K. Dwivedi, V.O. Pelenovich, X.Z. Zhao, W. Gao and D. Fu, *Sci. Rep.*, **8**, 10691 (2018); https://doi.org/10.1038/s41598-018-29025-1
37. H.B. Huang, Y. Wang, F.Y. Cai, W.B. Jiao, N. Zhang, C. Liu, H.L. Cao and J. Lu, *Front Chem.*, **5**, 123 (2017); https://doi.org/10.3389/fchem.2017.00123
38. S. Steplin Paul Selvin, A. Ganesh Kumar, L. Sarala, R. Rajaram, A. Sathiyan, J. Princy Merlin and I. Sharmila Lydia, *ACS Sustain. Chem.& Eng.*, **6**, 258 (2018); https://doi.org/10.1021/acssuschemeng.7b02335